Research Article
doi.org/10.1002/batt.202300313
Chemistry Europe
European Chemical Societies Publishing

www.batteries-supercaps.org

Path-Dependent Ageing of Lithium-ion Batteries and Implications on the Ageing Assessment of Accelerated Ageing Tests

Marcel Rogge*[a] and Andreas Jossen[a]

Path dependency in ageing of Lithium-ion batteries (LIBs) still needs to be fully understood, and gaps remain. For realistic operational scenarios that involve dynamic load profiles, understanding this path dependency is essential for effective monitoring and accurate modelling of LIBs-ageing. Our research investigates the impact of different ageing sequences on capacity reduction and resistance increase, key metrics for determining the state of health (SOH). Moreover, we argue that relying solely on SOH-based monitoring is insufficient for predicting the ongoing ageing trajectory. Our findings underscore that recent operational history influences subsequent degradation. This degradation is attributed to the emergence of uneven lithium distribution, which can both induce capacity recovery and amplify degradation during cycling phases. Such insights are particularly interesting for ageing studies where accelerated battery degradation is achieved through continuous cycling, a common approach in most cyclic ageing investigations. We demonstrate that capacity difference analysis (CDA) holds promise in tracking this unevenness and the potential for capacity restoration through re-homogenisation. In conclusion, our work highlights the importance of utilising advanced tools, such as CDA and degradation mode (DM) analysis, to ensure accurate conclusions are drawn in accelerated LIB-ageing experiments.

Introduction

LIBs (LIBs) undoubtedly have a decisive role in transitioning to a carbon-neutral future. One of the most crucial challenges for using LIBs lies in accurately estimating the SOH, typically determined as the residual capacity and/or rise in resistance in relation to their initial values. Accurate estimation of the SOH is especially crucial to ensure safe usage of LIBs over the lifetime and predict its end of life.[1] For this, ageing models are developed to depict the decay of LIBs in response to operational conditions and to provide a SOH as a measure for a LIBs age. As ageing models are hardly transferable between different types of LIBs, empirical studies are carried out to design proper ageing models, in most cases as isolated investigations for calendric[2–6] and cyclic ageing.[7–9] Besides depicting the course of ageing isolated for calendric and cyclic ageing, some studies try to create a combined model through a super positional approach,[10,11] where calendric and cyclic ageing is simply added. As many interacting processes are involved in battery ageing, such an approach is not sufficient.[12] More modern ageing models try to tackle these challenges. For example, based on the superposition approach from Schmalstieg et al.,[11] Hildenbrand et al.[13] extended the ageing model with an additional RC circuit and a voltage source to include reversible capacity loss and recovery effects caused by the anodic overhang. Another example is the work from Redondo-Iglesias et al.[14] who integrated a mechanism into their model, where the calendric ageing rate is not only influenced by temperature and state of charge (SOC) but also is modified by the cycling conditions.

Despite the many efforts made to assess and depict these complex interactions of LIB-ageing, the question of whether LIBs show a path dependency in ageing and how it can be integrated into a model needs to be revised. As no clear definition of path dependency concerning LIB-ageing exists, Röder et al.[12] gave different definitions of the path (in)dependency for the ageing of LIBs. Terms **PD I**, **PD II**, and **PD III** from their review on path dependence will further be used as they provide unambiguous definitions in the authors' view. **PD I** says that the operational conditions in general influence the ageing of LIBs. That means e.g. a cell which is constantly cycled will not age the same way as a similar cell, which only rests. **PD II** additionally says that the temporal sequence of operational condition impacts the ageing of LIBs. **PD III** says that even if the state (that is, e.g. the SOH) of two cells as well as the cumulative stress of their path (that is, the cells have experienced the same operational conditions) is the same their history impacts the course of further ageing, that is how the temporal sequence is ordered. To provide a clear idea of those definitions, they are schematically illustrated in Figure 1.

[a] *M. Rogge, Prof. Dr. A. Jossen*
Chair of Electrical Energy Storage Technology
School of Engineering and Design
Technical University of Munich
München (Germany)
E-mail: marcel.rogge@tum.de
Homepage: https //www.epe.ed.tum.de/en/ees/homepage/

Research Article
doi.org/10.1002/batt.202300313
Chemistry Europe
European Chemical Societies Publishing

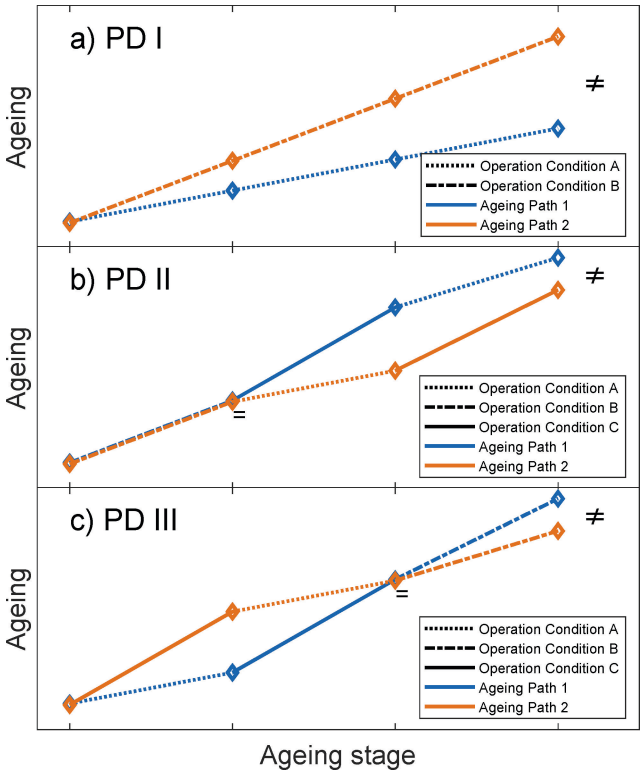

Figure 1. Definitions of path-dependent ageing of LIBs according to Röder et al.[12] **PD I** (a) only ascribes the operation condition as important for the ageing path, whereas **PD II** (b) does include the temporal sequence in which operation conditions are applied. **PD III** (c) says that even if the state (e.g. the SOH) is the same, the ageing history influences the further course of ageing.

The question of whether LIBs show a path dependency in ageing was already addressed in some studies. Gering et al.[17] conducted a study investigating whether different cycle profiles with the same cumulative energy-throughput lead to different ageing behaviours. The results from an early ageing stage indicated that constant current charging involves other ageing mechanisms when compared to constant power charging. To the authors' knowledge, further results from their continued study have yet to be published. Also, Klett et al. investigated LIBs-ageing under different ageing profiles.[18] For the constant current cycling, which showed the most severe ageing, as well as a hybrid electric vehicle inspired load profile, an inhomogeneous degradation of the negative electrode along the jelly roll could be observed. This was not the case for the calendrically aged cells, which showed very homogeneous ageing along the electrodes. They argued that those local phenomena observed for cells aged under cycling conditions are probably caused by the application of high-intensity loads and might be linked to path-dependent ageing. Su et al. analyzed, whether path dependency can be observed for calendric ageing conditions by varying the temporal sequence of applied ageing conditions.[16] In sum, all cells experienced the same cumulative amount of different ageing conditions. Lastly, no path dependency could be observed, with the exception that the resistance was slightly different for cells aged under different SOC ageing paths. Raj et al.[19] used a combination of calendric and cyclic ageing profiles to investigate the impact of sequences and the intensity of the ageing factor, in this case, the C-rate during cycling. The two groups of LIBs, aged with different ageing profile sequences but equally high C-rates, degraded differently. Through incremental capacity analysis (ICA) and differential voltage analysis (DVA), they reasoned a higher loss of lithiated active material at the negative electrode for the cells subjected to a more temporally dense cyclic ageing phase. They concluded that when continuous cycling is applied without more frequent interruptions for resting of the LIBs, cells might degrade faster. Similar to,[16] Werner et al.[15] concluded from their results that no path dependence could be observed for the sequence of different temperatures for calendric ageing. Karger et al.[20] investigated whether the charge throughput or the residual capacity shall be used to model the switching between ageing paths and if path independence can be assumed. From their results, they concluded that, on the one hand, the residual capacity is better suited to model the capacity fade. On the other hand, they see non-commutative ageing not as a definitive sign of path-dependent ageing. Instead, nonequal capacity fades for the same amount of ageing events (operational conditions), which qualifies **PD II**, might result from the sum of different sections of respective ageing trajectories. In their view, path dependency is only given when also a historical dependency, which means how the current ageing state is reached, impacts the further ageing (**PD III**). Liu et al. conducted two studies where they investigated the interaction of different ageing phases at different temperatures. In the first study,[21] cells were first cycled at low-temperature condition (−10 °C) until 90% or 80% SOH, and afterwards changed to high-temperature condition (50 °C) and compared to cells which have been aged at constant ageing condition (low or high temperature). Interestingly, they could observe accelerated ageing for cells, which have initially cycled at low temperatures, compared to the cells aged at constantly high temperatures. They argue that plated Li still present from low-temperature cycling accelerates SEI growth. In their second study,[22] cells were first cycled at high temperatures (50 °C) until they reached ~80% SOH and afterwards changed to low-temperature cycling conditions (−10 °C) and compared to the cells aged at constant ageing conditions. Interestingly, here, the ageing was decelerated in comparison to the cells aged under constant temperature conditions. These two studies show that not only the SOH is decisive for the further ageing rate but also the previous ageing history.

To further shed some light on the path dependency of LIB-ageing and how it impacts ageing the usability of accelerated ageing tests, our study focuses on the following questions:

F1 Does the sequence of ageing phases have an impact on the overall ageing, in the form of capacity fade or resistance increase, of LIBs (**PD II**)?

F2 Does the previous path (that means the different sequential order of operational conditions) impact the further course of ageing when the SOH is similar (**PD III**)?

Research Article
doi.org/10.1002/batt.202300313
Chemistry Europe
European Chemical Societies Publishing

F3 Is the SOH suitable for indicating the current ageing state, especially for ageing tests with continuous cycling conditions?

By answering these questions, we support the design of empirical ageing studies and models, which targets the depiction of ageing in application near scenarios with varying operating conditions. To find answers to these questions, this study is designed to apply an equivalent amount of stress factors, in the form of calendric and cyclic stress, in different temporal sequences. The sequences are chosen to give enough possibilities for comparing the different groups in their SOH and to draw conclusions if a path dependency is observable. Further, the results from SOH-assessment are evaluated and critically evaluated and classified.

Experiment & Methodology

Used cells and test-equipment

This study uses 18 commercially available high-energy INR 18650 35E cylindrical cells from Samsung SDI from the same delivery batch. The cells use NCA as positive, and a SiO/Gr-blend as negative active-material.[23,24] As in literature, different nominal capacities are mentioned between 3.35 Ah to 3.4 Ah,[25–27] we use 3.4 Ah as nominal capacity C_N for charge amounts and current rates throughout this study to avoid any confusion. The cells are divided into three groups with six cells each, whereas one group represent one of three chosen sequential permutation of ageing paths. We use six cells per ageing path to ensure that the conclusions made are statistically significant. BaSyTec Cell Test Systems (CTS) are used for cyclic ageing and reference performance test (RPT) procedure. For a controlled environment temperature during cycling and elevated temperatures during calendric ageing, Binder KT 115 climate chambers are used. Except for the calendric ageing phase where an ambient temperature of 45 °C is used, all tests and measurements are conducted at an ambient temperature set to 25 °C.

Description of the test procedures

To create a permutation in the sequence of ageing conditions, six ageing phases are defined of which two are cyclic ageing phases, further referred to as Cyc_1 and Cyc_2, and four are calendric ageing phases, further referred to as Cal_1 to Cal_4. To avoid erroneous conclusions due to non-subsided effects from the battery operation, an additional resting phase is appended after the six ageing phases to allow relaxation for all groups. This phase is further notified as *Rlx*. An overview of the overall test procedure, including the different ageing paths, is visualised in Figure 2, whereas the group experiencing the blue ageing path are further denoted as G_1, the group experiencing the orange path as G_2 and lastly, the group experiencing the green path as G_3. To capture the effects of the different phases, a RPT is carried out at the beginning of the experiment, at every ageing stage and at the end of the experiment. The points of time of the RPTs are denoted as t_{in}, t_1 to t_6 and t_{end}, respectively. As a general procedure, specific SOCs are always targeted Ah-based, which means, from a fully charged state, the cell is discharged with a C/3 current rate until the necessary capacity is discharged and the intended SOC is reached. The necessary discharge capacity is derived from the previous C/3 capacity measurement. To charge cells to 100% SOC, constant-current constant-voltage (CCCV) protocol is generally applied with

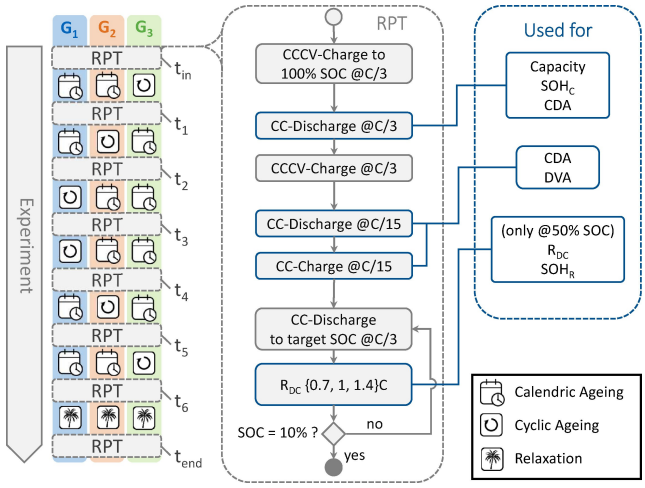

Figure 2. Overview of the experiment. The ageing of three groups, G_1 to G_3, differs in the temporal order of ageing phases, consisting of calendric ageing, cyclic ageing and a final relaxation phase. The ageing is captured in a reference performance test (RPT), which is conducted initially (t_{in}), after every ageing phase (t_1 to t_6) and at the end of the experiment (t_{end}). Data acquired from RPT are used for different analyses like SOH-determination or DVA.

a nominal current rate of C/3 until the end of charge voltage (U_{EOC}) voltage of 4.2 V is reached, and U_{EOC} is held until the current drops below 68 mA (or C/50). To capture the quasi open circuit voltage (qOCV), a current rate of C/15 is chosen. In many cases, this current rate might be seen as inadequate low for a qOCV. Nevertheless, rate tests for the full cell and the half-cell of the negative electrode have been performed beforehand to ensure that a suitable current rate for DVA is chosen. In the following sections, the single test procedures are described.

Reference Performance Test

At the beginning of any RPT procedure, the cell is fully charged. After 15 min rest, the discharge capacity is determined by discharging the cell with C/3 until 2.65 V (the end of discharge voltage (U_{EOD})) is reached. After 15 min rest, the cell is fully charged again. To obtain qOCVs, the cell is discharged afterwards with a current rate of C/15. After another rest of 15 min, the cell is recharged with C/15 until the U_{EOC} is reached. After a pause of 15 min, the cell is discharged Ah-based with C/3 to SOCs 90%, 50% and 10% for pulse resistance measurements. After reaching the intended SOC, the cell rests for 30 min before three pulses with 0.7C, 1C and 1.4C are applied for 20 s. For 90% SOC, only discharge and at 10% SOC, only charge-pulses are performed to avoid exceeding the voltage criteria. The charge throughput is compensated by the corresponding charge and discharge with C/6 to avoid the drift of SOC. For 50% SOC, the discharge pulses are followed by charge pulses with the same current rate; hence, no compensation is necessary. Between any two consecutive pulses, a pause of 5 min is applied to allow relaxation after compensation or the previous pulse.

Calendric ageing phase

Before the calendric ageing phase is started, cells are fully charged after the RPT via CCCV protocol with a current rate of C/3 to U_{EOC} and cutoff-current of C/50. Afterwards, the cells are discharged Ah-based with C/3 to 50% SOC with regards to the previously

determined C/3 discharge capacity. The storage SOC of 50% are chosen to minimise the effects of the anodic overhang as the mean SOC during the cyclic ageing phase is also at ~50%. After reaching the storage SOC, the cells are stored in an open circuit state for calendric ageing. One calendric ageing phase lasts for 35 days (or five weeks) with an ambient temperature of 45 °C.

Cyclic ageing phase

At the beginning of every cyclic ageing phase, the cells are fully charged, followed by a 30 min rest. After the rest, the cell is discharged to an upper target voltage U_{up}, which is 4.05 V for Cyc_1 and 4.1 V for Cyc_2, via CCCV with cutoff-current of C/50.

After a rest, 100 partial cycles are applied, whereas a partial cycle is conducted as follows: From the upper target voltage U_{up}, the cell is CC-discharged with 70% depth of discharge (DOD) with regards to C_N (2380 mAh) and a discharge current of ~0.9C (3020 mA). After discharge, the cell rests for 30 min and is charged via CCCV with a charging current of ~0.45C (1510 mA) to U_{up}. U_{up} is held until the current drops below C/50 or the CV phase lasts for 1 h. After another 10 min rest, the next partial cycle starts.

For Cyc_1, U_{up} is 4.05 V, which corresponds to ~83% SOC, and for Cyc_2, U_{up} is adapted to 4.1 V to avoid an exceed of U_{EOD} while cycling. 4.1 V correspond to ~90% SOC. As the DOD is 70%, the mean SOC is ~48% and ~55% during cycling respectively.

Final relaxation phase

As shown later in the results part, recovery effects are observed, which we will explain in the discussion part through the re-homogenisation of an inhomogeneous lithium distribution in the active material. As a consequence, an additional relaxation phase (notified as *Rlx*) is implemented at the end of the experiment to establish a homogeneous and comparable state between the different groups. Therefore the cells are fully charged after the last RPTs and are discharged to 50% SOC and rested for another five weeks at 25 °C at an open circuit condition before a final RPT is carried out.

Methodology

SOH evaluation

To evaluate whether path dependency can be observed, the common SOH-indicators capacity and resistance are consulted. As six cells are used for each group, SOH-values will be calculated individually, for the capacity calculated in Eq. (1):

$$SOH_C = \frac{C_{C/3}}{C_{C/3,ini}} \cdot 100\,\% \tag{1}$$

where $C_{C/3}$ is the current C/3 discharge capacity and $C_{C/3,ini}$ the initial C/3 capacity.

For the resistance, an increase by 100% is often regarded as the end-of-life criterion.[28,29] For simplicity, the SOH with regards to resistance SOH_R, will be defined as 100% initially and as 0%, when the resistance has increased by 100%. Hence, SOH_R is calculated through Eq. (2):

$$SOH_R = \left(1 - \frac{R - R_{ini}}{R_{ini}}\right) \cdot 100\,\% \tag{2}$$

Any statements about groups are always meant as the mean value of the six cells of the respective groups, e.g. in Eq. (3) for the capacitive SOH for G_1:

$$SOH_{C,G_1} = \frac{1}{6} \cdot \sum_{i=1}^{6} SOH_{C_i,G_1} \tag{3}$$

Any deviations provided for groups, e.g. error bars in plots, are calculated from the standard deviation as in Eq. (4):

$$\sigma = \sqrt{\frac{1}{6-1} \cdot \sum_{i=1}^{6} |x_i - \mu|^2} \tag{4}$$

where σ is the standard deviation, x_i the i-th value and μ the groups' average value.

Anodic overhang and inhomogeneity in lithium distribution

Multiple studies revealed possible recovery effects that can take place after the operation of LIBs, which can distort the analysis of the ageing behaviour, especially on the available capacity.[30,31] Among those distortions, the geometrical overlap of the negative electrode, commonly referred to as anodic overhang, is known to lead to falsified residual capacity measurements.[13,30] To reduce the effect of anodic overhang, SOCs are adjusted to be 50% during calendric ageing and relaxation as well as around 40% to 50% mean SOC during cycling to avoid long-lasting unequal SOCs between the anode overhang and the rest of the negative active material as good as possible.

Besides the anodic overhang, other effects might lead to a reversible loss of capacity, often attributed to inhomogeneous lithiation of the anodic active material.[32,33] Lewerenz et al.[34] observed a linkage between inhomogeneous lithiated graphite and difference in available capacity at different discharge rates, where the latter was introduced as CDA. CDA evaluates the difference between capacity measurements with different C-rates and has originally been used to quantify lateral current flow. To validate if CDA is suitable as a measure for recoverable capacity resulting from re-homogenisation, where a lateral flow in the active material can be expected, a correlation analysis between the capacity differences and observed capacity recoveries is carried out at the end of the study. The recovered capacity is defined as the difference in C/3 capacity from the RPT after a cyclic ageing phase and a consecutive calendric ageing or relaxation phase. Consequently, the recovered capacity C_{rec} can simply be calculated from the difference of the C/3 capacity $C_{C/3,cyc}$ after a cyclic ageing phase and the C/3 capacity $C_{C/3,\mathrm{cal}}$ from a consecutive calendric ageing phase as given in Eq. (5):

$$C_{rec} = C_{C/3,cyc} - C_{C/3,cal} \tag{5}$$

As mentioned, the CDA is defined as the difference in capacity between two capacity measurements with different current rates. As in our case, C/3 as well as C/15 discharge measurements are carried out, CDA value C_{CD} is obtained as given in Eq. (6):

$$C_{CD} = C_{C/15} - C_{C/3} \tag{6}$$

It is assumed that capacity might be recovered when inhomogeneities within the cell, such as an inhomogenous lithium distribution, cease. Hence, if there is a recovery caused by the cease of

inhomogeneity, a difference in CDA has to be observed and can be computed from Eq. (7):

$$\Delta C_{CD} = C_{CD,cyc} - C_{CD,cal} \tag{7}$$

To evaluate if capacity recovery is linked to a reduction in inhomogeneity, the linear correlation is evaluated through the calculation of the Pearson correlation coefficient[35] and calculated as in Eq. (8):

$$\rho(C_{rec}, \Delta C_{CD}) = \frac{cov(C_{rec}, \Delta C_{CD})}{\sigma_{C_{rec}} \cdot \sigma_{\Delta C_{CD}}} \tag{8}$$

Degradation modes analysis

In contrast to the typical usage of SOH to determine a LIBs current age, degradation modes provide more detailed information on the cause and effect of the battery ageing. The most common degradation modes describe the loss of cyclable lithium or loss of lithium inventory (LLI), the loss of active material at the positive electrode (LAM_{PE}) and loss of active material at the negative electrode (LAM_{NE}) and can be acquired through the fitting of the superpositioned half-cell qOCVs to the full-cell qOCV, or their respective derivatives obtained through DVA or ICA. The following describes the procedure to compute the degradation modes in this study. To obtain the half-cell qOCV of the negative electrode, a pristine cell has been disassembled in a glovebox under an argon atmosphere. Coin cells with Li counter-electrode have been assembled from the harvested electrode material. Based on the specific areal capacity of 4.89 $mAh\,cm^{-2}$ from,[36] coin cells have been initially cycled once with C/35, once with C/25 and finally with C/15 to obtain the half-cell qOCV for the intended rate. For the positive electrode, the qOCV for C/15 is provided by the ISEA institute of the RWTH Aachen University, which we gratefully acknowledge. The algorithm for calculating the DMs is adapted from Schmitt et al.,[37] whereas the general concept of determination of degradation modes through the mechanistic perspective of half-cell overlapping was introduced by Dubarry et al.[38] The current full-cell qOCV, U_{FC}, at a given full-cell SOC x_{FC} is the difference of the two half-cell qOCVs U_{NE} and U_{PE} at their respective SOCs x_{NE} and x_{PE} which is depicted in Eq. (9):

$$U_{FC}(x_{FC}) = U_{PE}(x_{PE}) - U_{NE}(x_{NE}) \tag{9}$$

Following the implications of Ref. [37], the half-cell SOCs x_{NE} and x_{PE} are linked to the full-cell SOC through Eq. (10):

$$x_{FC} = \alpha_{NE} \cdot x_{NE} + \beta_{NE} = \alpha_{PE} \cdot x_{PE} + \beta_{PE} \tag{10}$$

Where α_{NE} and α_{PE} are the scaling and $ß_{NE}$ and $ß_{PE}$ are the shift parameters for the negative electrode and the positive electrode, respectively. A half-cell's scaling factor is given as provided in Eq. (11):

$$\alpha_{HC} = \frac{C_{HC}}{C_{FC}} \tag{11}$$

Where C_{HC} is the respective half-cell capacity, C_{NE} for the negative electrode and C_{PE} for the positive electrode, and C_{FC} is the full-cell capacity. The shift parameter describes the absolute difference in the scaled half-cell SOC to the full-cell SOC and can be computed as in Eq. (12):

$$\beta_{HC} = x_{FC} - \alpha_{HC} \cdot x_{HC} \tag{12}$$

As the scale and shift parameters result from the fitting and C_{FC} is measured during the RPT, LAM_{PE} and LAM_{NE} can further be calculated as in Eq. (13) and Eq. (14):

$$LAM_{PE} = \frac{C_{PE,ini} - C_{PE}}{C_{PE,ini}} \tag{13}$$

$$LAM_{NE} = \frac{C_{NE,ini} - C_{NE}}{C_{NE,ini}} \tag{14}$$

Where $C_{PE,ini}$ and $C_{NE,ini}$ are the positive and negative electrodes' initial capacities, respectively. The LLI is described as the relative change in the amount of cyclable lithium, given in Eq. (15):

$$LLI = \frac{C_{Li,ini} - C_{Li}}{C_{Li,ini}} \tag{15}$$

Where $C_{Li,ini}$ is the initial amount of cyclable lithium and C_{Li} the amount of cyclable lithium at the time of the RPT, which is given through Eq. (16):

$$C_{Li} = C_{FC} \cdot (\alpha_{PE} - \alpha_{NE} + \beta_{PE}) \tag{16}$$

For a more detailed explanation of the previous equations, the reader is redirected to the publication of Schmitt et al.[37]

Experimental results

Course of capacity and resistance

In Figure 3(a), the C/3 discharge capacities of the three groups are plotted throughout the experiment. Initially, the average group capacities are (3328 ± 2) mAh. At the end of the experiment, groups 2 and 3 show nearly the same residual capacity with 3103 mAh and 3108 mAh on average. In contrast, the average residual capacity of G_1 is 3065 mAh. In means of SOH the average decrease is 6.77 % and 6.57 % for G_2 and G_3, whereas the SOH of G_1 is reduced by 7.97 % at the end of the study. Summarized, G_1 loses roughly 20 % more capacity than G_2 and G_3.

Figure 3(b) shows the course of resistance over the experiment. For simplicity, only discharge pulses at 50 % SOC with a current rate of 1C, evaluated at $\Delta t = 10$ s are regarded. G_1 initially shows a resistance of 37.1 mΩ. For G_2, resistance is 37.0 mΩ and for G_3, a resistance of 37.2 mΩ is determined. At the end of experiment measured resistances are 38.8 mΩ, 38.0 mΩ and 37.6 mΩ in average for G_1, G_2 and G_3, respectively. Hence the relative increase to their initial values are 4.46 % for G_1, 2.56 % for G_2 and 1.24 % for G_3. Consequently, G_1 shows a 74.2 % to 259.7 % higher resistance increase in comparison to G_2 and G_3. Nevertheless, these values have to be cautiously considered as the increase in resistance is moderate.

Research Article
doi.org/10.1002/batt.202300313
Chemistry Europe
European Chemical Societies Publishing

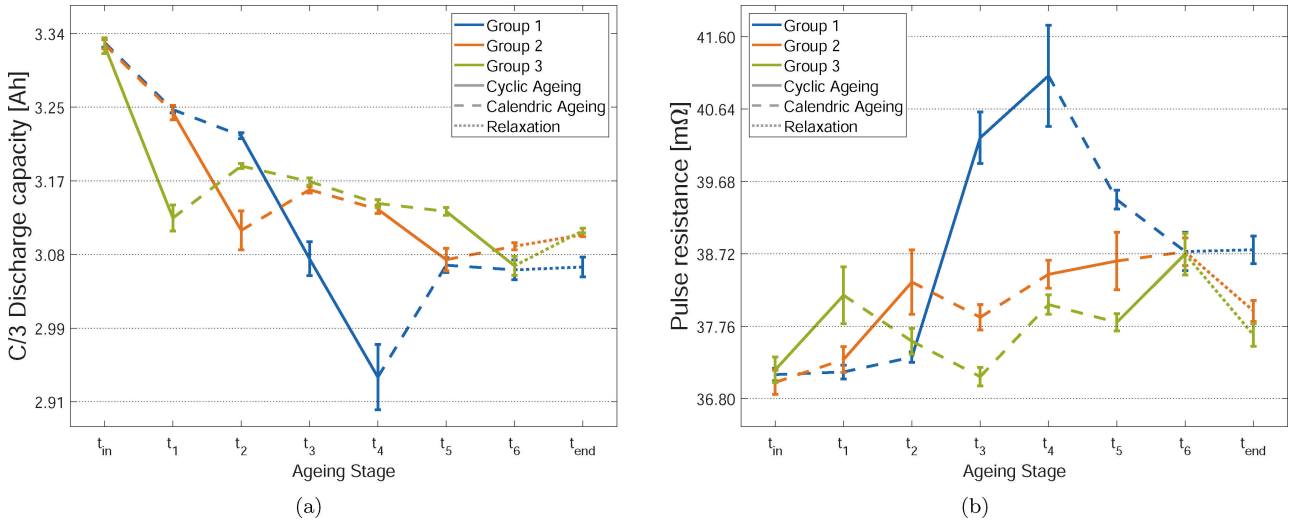

Figure 3. (a) Course of C/3 capacities over the experiment. Cyclic ageing phases, indicated through solid transition lines, lead to a high momentary capacity loss. Capacity is recovered in a consecutive calendric ageing phase, indicated through dashed transition lines. (b) Discharge pulse resistances acquired @ 50 % SOC and $\Delta t = 10$ s. Also, here, recovery is observable as a decrease in resistance.

Impact of ageing phases on capacity and resistance

To evaluate whether particular ageing phases have an equal impact on the groups, the phases are analysed regarding the change in capacity and resistance as shown in Figure 4. First, the effect on capacities of the groups, which are visualised in Figure 4(a), are considered.

Cyclic ageing phases, highlighted as solid lines in Figure 3(a), cause a higher momentary capacity decrease in comparison to calendric ageing phases. For G_1, the capacity loss amounts to 145.5 mAh and 139.9 mAh for Cyc_1 and Cyc_2 respectively. G_2 loses 139.3 mAh in Cyc_1 and 59.6 mAh in Cyc_2, whereas G_3 loses 203.6 mAh in Cyc_1 and 64.4 mAh in Cyc_2. Interestingly, the capacity loss in Cyc_1 is roughly 39.92 % and 46.15 % higher for G_3 in comparison to G_1 and G_2. Except for G_1, Cyc_2 shows a significantly lower capacity decrease. For G_1, the capacity decrease of Cyc_2 is nearly as high as in Cyc_1.

In the calendric ageing phases, the change in capacity highly depends on whether the calendric ageing phase follows a cyclic ageing phase. A capacity recovery instead of a loss can be observed for all calendric ageing phases following a cyclic ageing phase. E.g. for Cal_3 of G_1, which follows after two consecutive cycling phases, an average capacity increase of 132.3 mAh can be observed. Also for G_2, the average capacity increases by 48.1 mAh and 15.9 mAh in Cal_2 and Cal_4, whereas 61.4 mAh and 41.6 mAh are recovered in Cal_1 and Rlx of G_3.

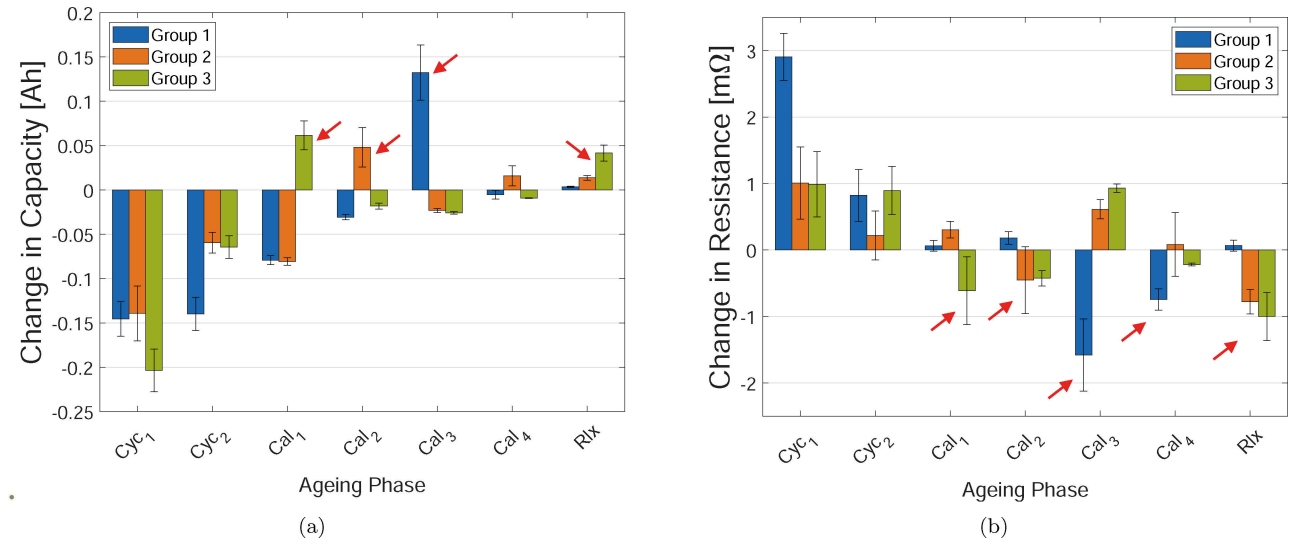

Figure 4. Impact of the cyclic ageing phases Cyc_1 and Cyc_2, calendric ageing phases Cal_1 to Cal_4 and relaxation phase Rlx on capacity (a) and resistance (b). G_3 shows the highest apparent capacity loss in Cyc_1 whereas for Cyc_2, G_1 loses more than twice the capacity compared to G_2 and G_3. In calendric ageing phases as well as in Rlx, recovery effects can be observed (highlighted by red arrows).

Research Article
doi.org/10.1002/batt.202300313
Chemistry Europe
European Chemical Societies Publishing

Consulting Figure 4(b) to analyse the effect of ageing phases on the resistance, differences are present compared to the course of capacity. For the capacity, Cyc_1 of G_3 shows the highest decrease, whereas for the resistance Cyc_1 of G_1 shows the highest increase with 2.90 mΩ. Roughly 3 times lower, the increase in resistance in Cyc_1 for G_2 and G_3 shows a very similar value with 1.01 mΩ and 0.99 mΩ respectively. Also, contrariwise to the capacity, Cyc_2 of G_1 does not increase the resistance as high as Cyc_1 but is much lower with 0.82 mΩ. Also, for G_2, the rise in resistance is significantly lower in Cyc_2 compared to Cyc_1. For G_3, the resistance increases in Cyc_2 by 0.89 mΩ and is therefore only slightly lower as in Cyc_1 with 0.99 mΩ.

In the calendric ageing phases, recovery effects can also be observed. Similar to the capacity, recovery in the form of reduction in resistance is observed in Cal_3 of G_1 where the resistance reduces by 1.58 mΩ over this phase. Also, for Cal_2 of G_2 and Cal_1 of G_3, a reduction of resistances can be observed, with differences of 0.45 mΩ and 0.61 mΩ measured to their previous checkup respectively. In contrast to the capacity, Cal_4 of G_2 shows no clear recovery as some cells have an increased resistance, some a reduced resistance and for some, only a marginal change can be observed. Interestingly, recovery effects (in the form of a reduction in resistance) occur beyond the first storage phase after a cyclic ageing phase. E.g. for Cal_4 of G_1, the resistance still reduces by 0.74 mΩ, although a significant recovery has been taking place in the previous calendric ageing phase. The same behaviour can be observed for Cal_2 of G_3, still showing a decrease in resistance of 0.42 mΩ, although 0.61 mΩ has been recovered in Cal_1. Somehow unexpected is the decrease for G_3 in Cal_4 since in the previous ageing phase Cal_3, an increase in resistance has been observed.

Differential voltage and degradation modes analysis

Besides capacity and resistance, the DVA provides further insights into the degradation mechanisms that occur during ageing. Figure 5(a) shows the course of the DVAs derived from the C/15-charging qOCV over the different ageing phases for one cell of G_1, G_2 and G_3. At first glance, the DVAs of the different groups look similar at the end of the experiment. Besides a general shift to lower SOCs, the positive electrode features show no noticeable signs of change throughout the experiment. Contrariwise, negative electrode features do significantly change, especially during cyclic ageing phases. The most notable change is the disappearance of the central

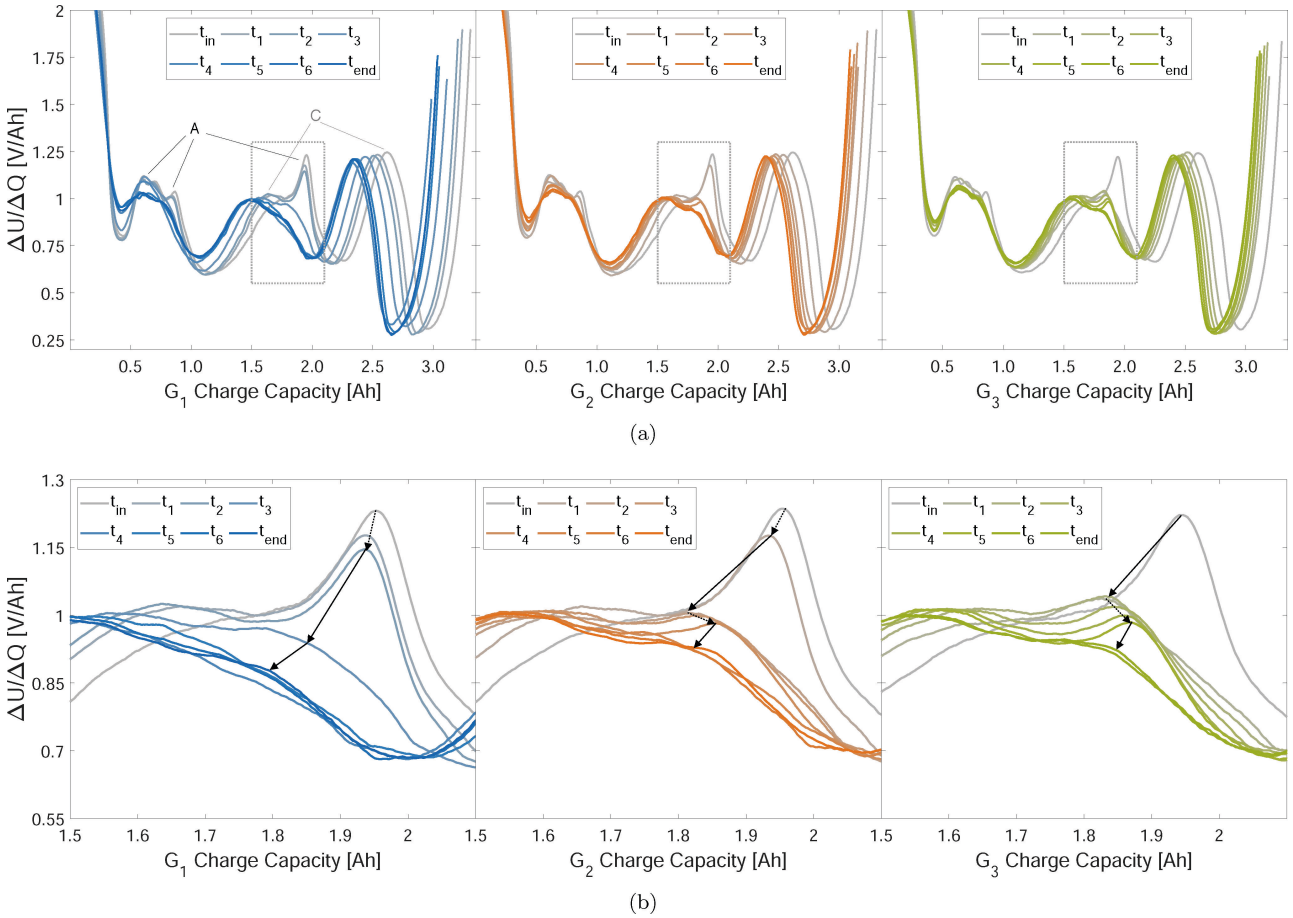

Figure 5. Evolution of DVA over the course of experiment (a). The impact on the main graphite peak is highlighted in (b), whereas the impact of cyclic and calendric ageing phases are marked as solid and dotted arrows, respectively. Generally, cycling leads to the "smearing" of negative electrode features ("A" in the left axis of (a)), whereas the positive electrode features ("C" in the left axis of (a)) are shifted towards lower SOCs. Calendric ageing causes a shift of positive and negative electrode features to each other, reasoning LLI as the dominant ageing effect.

graphite peak at ~2.0 Ah, which seems to disappear as soon as the first cyclic ageing phase is conducted. The central graphite peak is associated with the phase transition of graphite from LiC_{12} to LiC_6. Not only does the central graphite peak disappear, but also other negative electrode features, present at roughly 0.5 Ah to 1.0 Ah, get "smeared". In literature, the effect of vanishing and broadening peaks in DV and IC curves is attributed to an uneven distribution of lithium in the active material,[33,39,40] here specifically in the negative electrode. The smeared DVA can be understood as a superposition of DVAs of inhomogeneous lithiation, in this case, of the negative active material.

An inhomogeneous lithium distribution can occur in several ways. Well-known is the effect of the anodic overhang, where negative electrode active material without a positive electrode counterpart acts as a lithium sink or source, depending on its SOC and the SOC of the negative electrode material with a positive electrode counterpart.[41] Furthermore, an inhomogeneous lithiation of the negative electrode has been observed in the through-plane direction (that means in the direction from the separator to the current collector),[42] which e.g. can arise through preferable intercalation of lithium into the negative active material next to the separator during the charging process as the diffusion paths are shorter. Furthermore, an in-plane (that means along the surface of the electrode sheet) inhomogeneity has also been reported.[43] Such inhomogeneity might arise for different reasons,[32] such as an inhomogeneous current distribution,[43] temperature gradients[44] or pressure gradients.[45] In contrast to the cyclic ageing phases, the calendric ageing phases only slightly influence the height and prominence of features in the DVA. Looking at the change in DVA shapes of G_3 from checkups t_1 to t_5 in Figure 5(a), one can see that in the calendric ageing, the central graphite peak slightly "wanders" in the direction of higher SOCs whereas the positive electrode features shifts towards lower SOCs. This change in the offset of the two half-cells indicates LLI.[46]

Extrema in the full-cell DVA can be used to fit the half-cell DVAs and thereby obtain the degradation modes.[47] Figure 6 outlines the results from DM analysis, obtained through the automated fitting of DVAs. Due to an error in the synchronisation between the test device and the host system, data of the qOCVs measurements with C/15 for G_1 at t_5 are lost. Only the charge throughput could be recovered, but not the voltage course. Consequently, DMs cannot be derived for G_1 at t_5.

The general low change in positive electrode capacities, given as LAM_{PE}, is consistent with findings from visual inspection of the DVAs, where positive electrode features only shift towards lower SOCs and do not change in their scaling. LAM_{PE} reaches a maximal value of 4% at t_4 for G_1. For all three groups, the estimated positive electrode capacity is reduced only by ~1% at t_{end}. In contrast, LAM_{NE} seems to reach quite high values of up to 12.5% for G_1 at t_4. The increase in LAM_{NE} occurs only during cyclic ageing phases. For all groups, LAM_{NE} increases 6.2% to 7.0% within Cyc_1. In Cyc_2, LAM_{NE} increases by 4.8% to 5.8%. Although LAM_{NE} is not directly observable as capacity loss, since an underbalanced negative electrode ultimately leads to Li-plating, and hence LLI,[40] the higher LAM_{NE} of G_1 at the beginning of Cyc_2 might explain the higher capacity loss of G_1 in Cyc_2 compared to G_2 and G_3, as visible in Figure 4(a). Also noticeable is an increase in the deviation between the individual cells within a group as soon as cycling takes place. Before the Cyc_1, standard deviations have been 0.13% for G_1 and 0.35% for G_2 (for G_3 no deviation is present as only the initial checkup has been carried out before the Cyc_1, which is the reference for the calculation of LAM_{NE}). After Cyc_1, the deviations increase to 0.67%, 1.67% and 1.23% for G_1 to G_3, and reach 1.87%, 2.41% and 1.99% after Cyc_2 respectively. In general, calendric ageing phases only marginally increase the LAM_{NE}. Instead, LAM_{NE} is reduced in a calendric ageing phase if a cyclic ageing phase has been conducted beforehand. In contrast to the capacity recovery, the recovery for LAM_{NE} does not subside within the experiment, even after 4 phases of calendric ageing (G_3, Cal_1–Cal_4), which equals 20 weeks of rest. Consistent with the findings of capacity decrease and resistance increase, G_1 ageing differs from G_2 and G_3. G_1 lastly seems to lose ~9.1% of its initial negative electrode capacity, whereas G_2 and G_3 finally lose 6.9% and 7.8% of their initial negative electrode capacity respectively. The difference between G_1 to G_2 and G_3 can also be observed for the LLI. LLI of G_1 lastly reaches

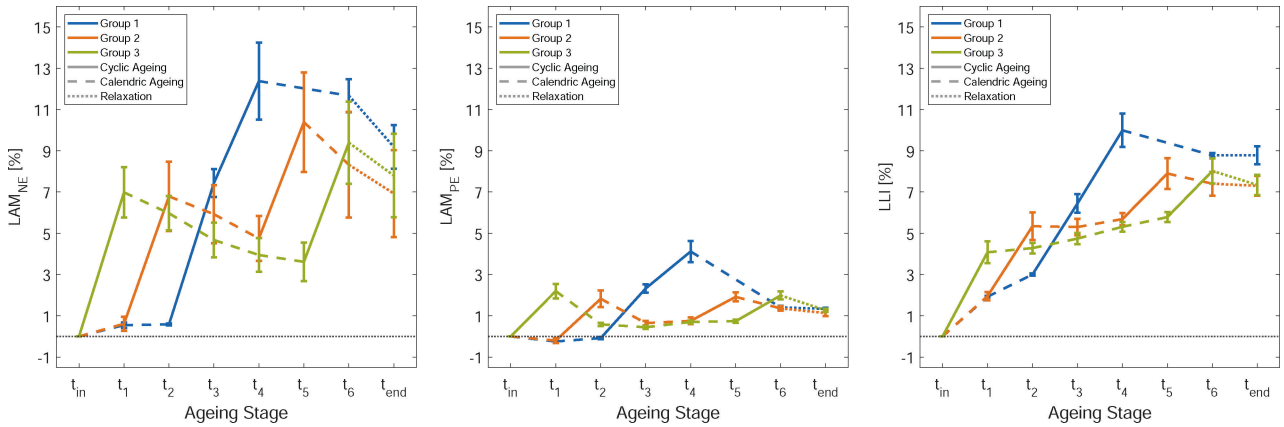

Figure 6. Degradation modes obtained through the fitting of half-cell DVAs to measured full-cell DVAs. LAM_{NE} and LLI are assumed to be the dominating ageing effects.

8.8%, whereas G_2 and G_3 both have lost 7.3% of their initial lithium inventory. Consequently, LLI is 20% higher for G_1.

Discussion

Path dependency in ageing

To answer the question of whether the sequence of ageing phases impacts overall ageing (**F1**), the available residual capacity and the increase in resistance, typically used for the definition of SOH, will be consulted. With the results presented, we see clear indications of path-dependent ageing. At the end of the experiment, the capacity loss of G_1 is 17.8% and 21.3% higher than the capacity losses of G_2 and G_3 respectively. Furthermore, the increase in pulse-resistance for G_1 is 74.2% and 259.7% higher in comparison to G_2 and G_3 respectively. However, the maximal relative increase in resistance is 9.6% for G_1 at t_4, and hence small changes have a high relative impact. Nevertheless, at t_{end}, any short-term effects subsided as the cells were allowed to relax for five weeks. Hence, the criterion for a path dependency of sequence, **PD II**, is clearly fulfilled. The answer to the question of whether a historical path dependency is given (**F2**) is not as straightforward as the previous one. Some aspects speak for the fulfilment of **PD III**. In Table 1, the ageing trends of groups are compared if the following conditions are met:

1. At t_x, the groups have experienced the same number of calendric and cyclic ageing phases but different ageing paths.
2. The groups will experience the same ageing/relaxation phase as the next phase.
3. The considered SOHs are comparable.

The SOH of two groups is regarded as comparable when the difference in their mean SOH-value is smaller than 0.5%. Further **PD III** is regarded as fulfilled when the difference in ageing trend between the groups regarded groups G_n and G_m, as calculated in Eq. (17):

$$\Delta SOH_{\Delta n \Delta m} = \left|\Delta SOH_{G_n} - \Delta SOH_{G_m}\right| \tag{17}$$

is higher as the highest standard deviation of the groups SOH at t_x. Expressed in a mathematical way **PD III** is met when condition in Eq. (18) is true:

$$\Delta SOH_{\Delta n \Delta m} > max\left(\sigma\left(SOH_{G_{n/m},t_x}\right)\right) \tag{18}$$

The ageing trend ΔSOH_{G_n} of a group G_n from t_x to t_y is calculated as in Eq. (19):

$$\Delta SOH_{G_n} = SOH_{G_n,t_y} - SOH_{G_n,t_x} \tag{19}$$

In four cases in Table 1, the criterion for **PD III** is met. In the first case G_1 and G_2 are compared for the ageing between t_5 and t_6 where SOHs are 92.1% and 92.3% at t_5, respectively. G_1 reached through calendric ageing whereas G_2 reached t_5 through cyclic ageing. From t_5 to t_6 the SOH of G_1 slightly decreases by 0.2% from 92.1% to 91.9% SOH, whereas the SOH of G_2 increases by 0.5% from 92.3% to 92.8%.

In the next case starting from ageing stage t_6, SOH of G_1 marginally increases by 0.1% to 92% until t_{end}, whereas the SOH of G_3 increases by 1.2% from 92.2% to 93.4%. Here again, G_1 reached t_6 trough calendric ageing, whereas G_3 reached t_6 through cyclic ageing.

In the third case, also starting from t_6, a divergence in ageing between G_1 compared to G_2 is present when the resistive SOH is considered. While G_1 have a SOH_R of 95.5% and, 95.2% for G_2, different ageing trends can be observed. For G_1, a small reduction can be observed. Contrariwise, for G_2 the SOH_R increases by 2.1%.

The same difference in ageing trends can be observed in the last case, where G_1 is compared to G_3 at t_6. While G_1 has a SOH_R of 95.5% and G_2 a SOH_R of 95.8%, the SOH_R of G_2 increases by 2.7% whereas the SOH_R of G_1 decreases by 0.2%.

From these four cases, we see that although nearly the same SOH is given and the following operational condition is the same, the ageing trend or magnitude can differ significantly. Contrariwise to the four cases shown, the ageing trends of G_2 and G_3 for the ageing phase between t_3 to t_4 are very similar. Starting from SOHs 94.8% and 95.2% for G_2 and G_3, the SOHs reduces by 0.7% and 0.8% for G_2 and G_3 respectively. In this case, G_2 as well as G_3 reached t_3 through a calendric ageing phase.

Table 1. Evaluation of historical path dependency (**PD III**) through the SOHs of G_1 to G_3. Assessment for the groups is performed at the ageing stage t_x when: 1. the regarded groups have experienced the same number of calendric and cyclic ageing phases but different ageing paths, 2. the same procedure (calendric, cyclic or relaxation phase) is conducted from t_x to t_y 3. the regarded SOHs are nearly equal at t_x ($\Delta \leq 0.5\%$). **PD III** is assumed to be qualified when the difference between the ageing trends ($\Delta SOH_{\Delta n \Delta m}$) is higher than the highest standard deviation of the regarded SOHs at t_x. A † as superscript means that the capacitive SOH is regarded, whereas a * superscript means that the resistive SOH is considered.

$t_x \rightarrow t_y$	Groups	$SOH_{C\dagger/R^*}$ @t_x	$SOH_{C\dagger/R^*}$ @t_y	$\Delta SOH_{\Delta n \Delta m}$	σ(SOH) @t_x	**PD III**
$t_3 \rightarrow t_4$	G_2/G_3	$94.8^{\dagger}/95.2^{\dagger}$	$94.1^{\dagger}/94.4^{\dagger}$	0.1	0.2/0.2	no
$t_5 \rightarrow t_6$	G_1/G_2	$92.1^{\dagger}/92.3^{\dagger}$	$91.9^{\dagger}/92.8^{\dagger}$	0.7	0.3/0.5	yes
$t_6 \rightarrow t_{end}$	G_1/G_3	$91.9^{\dagger}/92.2^{\dagger}$	$92.0^{\dagger}/93.4^{\dagger}$	1.1	0.4/0.5	yes
$t_6 \rightarrow t_{end}$	G_1/G_2	95.5*/95.2*	95.3*/97.3*	2.3	0.8/0.5	yes
$t_6 \rightarrow t_{end}$	G_1/G_3	95.5*/95.8*	95.3*/98.5*	2.9	0.8/1.1	yes

Research Article
doi.org/10.1002/batt.202300313
Chemistry Europe
European Chemical Societies Publishing

Obviously, the ageing trends of G_2 and G_3 are more similar than e.g. G_1 and G_2 or G_1 and G_3. Like Raj et al.[19] concluded that accelerated degradation for continuous cycling might take place; we also believe that G_1 differs in its ageing and degrades faster because the second cyclic ageing phase Cyc_2 is directly applied after the first cyclic ageing phase Cyc_1. The fact that Cyc_2 is detrimental for G_1 might be explained through a higher inhomogeneity in lithium distribution at the start of Cyc_2.

Impact of inhomogeneity on ageing evaluation & the promising tool CDA

The occurrence of a inhomogeneous lithium distribution have been reported[32,48,50] and explained.[18,43] As described in the methodology part, the experiment was designed to minimize the effect of the anodic overhang. Therefore, we assume that the main driver of the observed recovery effects is given through the re-homogenization of inhomogeneous lithium distribution in the negative active material. This assumption was also hypothesized by Morales et al., which observed even more significant recovery for the battery from the same type (Samsung 35E). The assumption is supported by the findings from the DVA section. Figure 7 plots the CDA, calculated from the difference between C/15 and C/3 capacity measurement, for G_1 to G_3 over the course of the experiment. Initially at ~0.04 Ah, the capacity difference (CD) reaches values up to ~0.14 Ah for G_1 after Cyc_2 (at t_4). Here we also can reason why Cyc_2 is more severe for G_1 compared to G_2 and G_3. At the beginning of Cyc_2 for G_2 (at t_4) and G_3 (at t_5), their CD value is between ~0.05 Ah to ~0.06 Ah, which indicates that a somehow homogeneous lithium distribution is present. In contrast, CD of G_1 is 0.11 Ah high at the beginning of Cyc_2 (at t_3). Since less capacity of the active material is contributing during the Cyc_2, where a discharge rate of ~0.9C and a charge rate ~0.45C is applied, less active material contributes to the de-/intercalation reaction, as it can be seen from LAM_{NE} and LLI in Figures 6 and 7. Therefore, higher current rates are present for the participating active material, coupled with higher stress through faster volume changes due to faster de-/intercalation of Li-ions. The higher mechanical stress ultimately can lead to higher irreversible LAM_{NE} and LLI through cracking of the negative electrode material, loss of electrical contact[51] and reformation of the solid electrolyte interface,[52] especially if the material is lithiated at the time of fatigue and it's Li-reservoir get isolated. This mechanism might reason the higher LLI for G_1 in Cyc_2 plotted in Figure 6. This mechanism of an increased local current density could further explain why continuous cycling at a certain point leads to more severe damage, accelerating the ageing of LIBs.

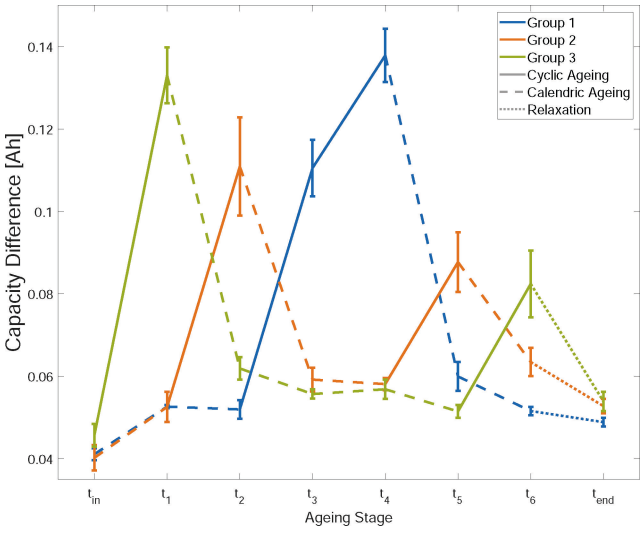

Figure 7. Capacity differences (CD) of groups G_1 to G_3. Cyclic ageing phases cause a temporary increase in CD, which disappears after a consecutive calendric ageing or relaxation phase. The reduced CD can explain an increased capacity measured after the consecutive calendric or relaxation phase, as an increased CD means less capacity can be extracted during C/3 measurement. An increased inhomogeneity in lithium distribution might be the reason for the increased CD.

Here, the non-subsided effects do not only cause path-dependent ageing by increasing the severeness of cycling for G_1 in Cyc_2, but also might lead to falsified statements on the current age of a LIB. Table 2 exemplary evaluates the capacity loss, which is equal to a decrease in SOH, of the three different groups at the different stages of the experiment and makes a qualitative statement regarding the ageing of the groups to each other. As one can see from the results, misjudges of individual ageing are the consequence. If, e.g. t_2 of G_2 and G_3 is regarded, the ageing of G_2, visible as capacity loss, will be interpreted as much higher than G_3. At this point, G_2 seems to have lost 55% more capacity than G_3. Comparing those two groups at stage t_3, the difference nearly disappears, even though the same stress has been applied to both of them. If G_1 is additionally considered at this stage, G_1 seems to have aged 50% more than G_2 and G_3. Looking at t_5, where G_1 and G_2 have seen the same cumulative stress, those two groups only slightly differ in their capacities. Throughout the rest of the experiment, this difference increases, although the applied ageing stress is the same for both groups.

We see that those misjudges are linked to the history dependency, which has been highlighted in the previous section. Clearly, a scalar SOH is not suited to reflect the current state of a battery with means of health and predictable ageing, but the recent history has to be considered. As one can see

Table 2. Qualitative comparison of the capacity loss at different ageing stages t_x. E.g. $X > Y$ means X showed a higher capacity loss (or apparent ageing) as Y, whereas $X < Y$ means X showed a lower capacity loss as Y. Comparisons at t_x are only conducted when groups experience the same stress, which means the same number of calendric and cyclic ageing phases.

t_x	Group 1		Group 2		Group 3
t_1	G_1	=	G_2		
t_2			G_2	>	G_3
t_3	G_1	>	G_2	≥	G_3
t_4			G_2	=	G_3
t_5	G_1	≥	G_2		
t_6	G_1	>	G_2	<	G_3 ($\leq G_1$)
Rlx	G_1	>	G_2	≥	G_3

Research Article
doi.org/10.1002/batt.202300313
Chemistry Europe
European Chemical Societies Publishing

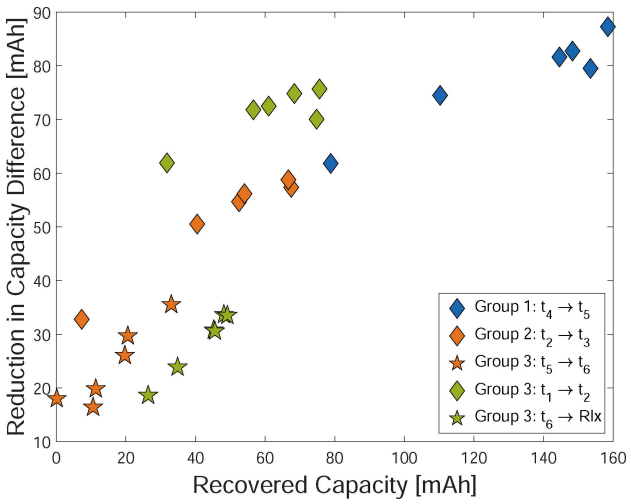

Figure 8. Correlation of reduction in capacity difference (CD) and recovered capacity. The high Pearson's ρ of 0.841 and low p-value of $5.88 \cdot 10^{-9}$ show that a high likeliness is given that a change in capacity difference and a change in recoverable capacity occur simultaneously. Based on this, CDA might be seen as a promising tool to monitor recoverable capacity.

from Figure 7, CDA seems to contain information about the recent cyclic stress history of the groups. After every cyclic ageing phase, the CD increases and decreases afterwards when no further cycling is conducted, and cells can homogenise. Since homogeneous lithiated cells show a higher C/3 capacity than inhomogeneous ones, a rehomogenisation shall be observable as an increase in available C/3 capacity, interpreted as a capacity recovery.

To examine the assumption that CDA can be used to approximate a recoverable capacity, a correlation between the difference in CD according to Eq. (7) and recovered capacity according to Eq. (5) is carried out. As visible in Figure 8, a high correlation is given with Pearson's ρ of 0.841[35] where a coincidence of correlation can be excluded with the given p-value of $5.88 \cdot 10^{-9}$ over all data points. The correlation does not imply that the reduction of CD is causal for the capacity recovery (or vice versa). But it shows that the change in CD and the change in recoverable capacity will likely occur together. Interestingly, a small decrease in CD is also observed between t_4 and t_5 of G_3. Probably, the decrease in CD can be related to the decrease in resistance for the same period of G_3, which initially could not be explained previously in the results section. Unfortunately, a mechanistic explanation cannot be given at this point. Nevertheless, including CDA is beneficial as it might serve as an indicator (or even a measure) for a present inhomogeneous lithium distribution and likeliness of recoverable capacity.

Conclusions

In this work, a study was conducted to answer three questions:

F1 Does the sequence of ageing phases have an impact on the overall ageing, in the form of capacity fade or resistance increase, of LIBs (**PD II**)?

F2 Does the previous path (that means the different sequential order of operational conditions) impact the further course of ageing when the SOH is similar (**PD III**)?

F3 Is the SOH suitable for indicating the current ageing state, especially for ageing tests with continuous cycling conditions?

Our results show that the sequence of ageing phases can have an impact on the overall ageing of LIBs. G_1, which experienced two consecutive cycling phases, show signs of higher degradation, not only in the form of a higher capacity decrease and resistance increase but also in the form of a higher LAM_{NE} and LLI.

Furthermore, we see a clear indication that the recent history impacts the further course of ageing, as the ageing of groups in some cases diverges for the same operational stress although they started from a similar SOH. Nevertheless, this divergence, as well as the difference in ageing paths, is probably driven by temporary effects, namely an inhomogeneous lithium distribution.

If inhomogeneous lithium distribution caused by cycling of the cells is present, recovery of capacity is measurable if the LIBs are allowed to re-homogenise. This makes it hard to describe a LIBs current age solely from the SOH since the recent operation history and expectable capacity recovery are not included. Hence, the SOH alone is insufficient to indicate the current state of LIBs, especially if dynamic operational conditions consisting of cycling and resting phases are applied.

Instead, further analysis has to be integrated into the test procedure, especially during ageing tests, which accelerates ageing through continuous cycling. In our case, capacity difference analysis (CDA) significantly correlates with capacity, which can be recovered in a phase of relaxation. Motivated by our results which show that inhomogeneous lithium distribution might cause path-dependent ageing as well as falsified ageing determination, we encourage further research on the impact of inhomogeneous lithium distribution on ageing paths, ageing evaluation and the development of tools to sufficiently monitor these inhomogeneities, such as CDA.

Acknowledgements

The authors gratefully acknowledge the financial support by the Federal Ministry of Education and Research, Germany, through the project BALd (BMBF, Grant Nr. 03XP0320B). Special thanks also go to Meinert Lewerenz, Pablo Morales Torricos and Alexander Karger for valuable discussions. Open Access funding enabled and organized by Projekt DEAL.

Conflict of Interests

The authors declare no conflicts of interests.

Data Availability Statement

The data that support the findings of this study are available from the corresponding author upon reasonable request.

Keywords: capacity difference analysis · degradation modes · electrochemistry · energy conversion · inhomogeneous lithium distribution

[1] H. Tian, P. Qin, K. Li, Z. Zhao, *J. Cleaner Prod.* **2020**, *261*, 120813.
[2] P. Keil, S. F. Schuster, J. Wilhelm, J. Travi, A. Hauser, R. C. Karl, A. Jossen, *J. Electrochem. Soc.* **2016**, *163*, A1872.
[3] P. Keil, A. Jossen, *J. Electrochem. Soc.* **2017**, *164*, A6066.
[4] M. Naumann, M. Schimpe, P. Keil, H. C. Hesse, A. Jossen, *J. Energy Storage* **2018**, *17*, 153.
[5] A. Karger, J. Schmitt, C. Kirst, J. P. Singer, L. Wildfeuer, A. Jossen, *J. Power Sources* **2023**, *578*, 233208.
[6] E. Redondo-Iglesias, P. Venet, S. Pelissier, *J. Energy Storage* **2017**, *13*, 176.
[7] T. R. Ashwin, Y. M. Chung, J. Wang, *J. Power Sources* **2016**, *328*, 586.
[8] Y. Wu, P. Keil, S. F. Schuster, A. Jossen, *J. Electrochem. Soc.* **2017**, *164*, A1438.
[9] M. Naumann, F. B. Spingler, A. Jossen, *J. Power Sources* **2020**, *451*, 227666.
[10] E. Sarasketa-Zabala, E. Martinez-Laserna, M. Berecibar, I. Gandiaga, L. M. Rodriguez-Martinez, I. Villarreal, *Appl. Energy* **2016**, *162*, 839.
[11] J. Schmalstieg, S. Käbitz, M. Ecker, D. U. Sauer, *J. Power Sources* **2014**, *257*, 325.
[12] F. Röder, S. Ramasubramanian, *Energy Technol.* **2022**, *10*, 2200627.
[13] F. Hildenbrand, D. Ditscheid, E. Barbers, D. U. Sauer, *Appl. Energy* **2023**, *332*, 120395.
[14] E. Redondo-Iglesias, P. Venet, S. Pelissier, *Batteries* **2020**, *6*, 14.
[15] K. L. Gering, S. V. Sazhin, D. K. Jamison, C. J. Michelbacher, B. Y. Liaw, M. Dubarry, M. Cugnet, *J. Power Sources* **2011**, *196*, 3395.
[16] M. Klett, R. Eriksson, J. Groot, P. Svens, K. Ciosek Högström, R. W. Lindström, H. Berg, T. Gustafson, G. Lindbergh, K. Edström, *J. Power Sources* **2014**, *257*, 126.
[17] L. Su, J. Zhang, J. Huang, H. Ge, Z. Li, F. Xie, B. Y. Liaw, *J. Power Sources* **2016**, *315*, 35.
[18] T. Raj, A. A. Wang, C. W. Monroe, D. A. Howey, *Batteries & supercaps* **2020**, *3*, 1377.
[19] D. Werner, S. Paarmann, T. Wetzel, *Batteries* **2021**, *7*, 28.
[20] A. Karger, L. Wildfeuer, D. Aygül, A. Maheshwari, J. P. Singer, A. Jossen, *J. Energy Storage* **2022**, *52*, 104718.
[21] J. Liu, Y. Zhang, J. Bai, L. Zhou, Z. Wang, *Electrochim. Acta* **2023**, *454*, 142362.
[22] J. Liu, L. Zhou, Y. Zhang, J. Wang, Z. Wang, *J. Cleaner Prod.* **2023**, *423*, 138678.
[23] H. Popp, N. Zhang, M. Jahn, M. Arrinda, S. Ritz, M. Faber, D. U. Sauer, P. Azais, I. Cendoya, *Elektrotech. Inftech.* **2020**, *137*, 169.
[24] F. C. Krause, J. P. Ruiz, S. C. Jones, E. J. Brandon, E. C. Darcy, C. J. Iannello, R. V. Bugga, *J. Electrochem. Soc.* **2021**, *168*, 040504.
[25] P. Berg, M. Spielbauer, M. Tillinger, M. Merkel, M. Schoenfuss, O. Bohlen, A. Jossen, *J. Energy Storage* **2020**, *31*, 101499.
[26] M. E. Wojtala, F. B. Planella, A. A. Zulke, H. E. Hoster, D. A. Howey, Investigating changes in transport, kinetics and heat generation over NCA/Gr-SiOx battery lifetime, in 2022 IEEE Vehicle Power and Propulsion Conference (VPPC), IEEE 01.11.2022–04.11.2022, pages 1–6.
[27] Samsung SDI, Specification of Product for Lithium-ion rechargeable cell Model name INR18650-35E **2015**.
[28] M. Ecker, J. B. Gerschler, J. Vogel, S. Käbitz, F. Hust, P. Dechent, D. U. Sauer, *J. Power Sources* **2012**, *215*, 248.
[29] T. Grandjean, J. Groenewald, A. McGordon, W. Widanage, J. Marco, *Batteries* **2018**, *4*, 49.
[30] R. Burrell, A. Zulke, P. Keil, H. Hoster, *J. Electrochem. Soc.* **2020**, *167*, 130544.
[31] B. Epding, B. Rumberg, H. Jahnke, I. Stradtmann, A. Kwade, *J. Energy Storage* **2019**, *22*, 249.
[32] F. B. Spingler, M. Naumann, A. Jossen, *J. Electrochem. Soc.* **2020**, *167*, 040526.
[33] M. Lewerenz, P. Dechent, D. U. Sauer, *J. Energy Storage* **2019**, *21*, 680.
[34] M. Lewerenz, S. Käbitz, M. Knips, J. Münnix, J. Schmalstieg, A. Warnecke, D. U. Sauer, *J. Power Sources* **2017**, *353*, 144.
[35] J. Cohen, Statistical power analysis for the behavioral sciences, Erlbaum, Hillsdale, NJ, 2. ed. edition **1988**.
[36] P. Kuntz, O. Raccurt, P. Azaïs, K. Richter, T. Waldmann, M. Wohlfahrt-Mehrens, M. Bardet, A. Buzlukov, S. Genies, *Batteries* **2021**, *7*, 48.
[37] J. Schmitt, M. Schindler, A. Oberbauer, A. Jossen, *J. Power Sources* **2022**, *532*, 231296.
[38] M. Dubarry, C. Truchot, B. Y. Liaw, *J. Power Sources* **2012**, *219*, 204.
[39] J. P. Fath, D. Dragicevic, L. Bittel, A. Nuhic, J. Sieg, S. Hahn, L. Alsheimer, B. Spier, T. Wetzel, *J. Energy Storage* **2019**, *25*, 100813.
[40] M. Dubarry, D. Anseán, *Front. Energy Res.* **2022**, *10*, https://doi.org/10.3389/fenrg.2022.1023555.
[41] B. Gyenes, D. A. Stevens, V. L. Chevrier, J. R. Dahn, *J. Electrochem. Soc.* **2015**, *162*, A278.
[42] D. P. Finegan, A. Quinn, D. S. Wragg, A. M. Colclasure, X. Lu, C. Tan, T. M. M. Heenan, R. Jervis, D. J. L. Brett, S. Das, T. Gao, D. A. Cogswell, M. Z. Bazant, M. Di Michiel, S. Checchia, P. R. Shearing, K. Smith, *Energy Environ. Sci.* **2020**, *13*, 2570.
[43] A. Senyshyn, M. J. Mühlbauer, O. Dolotko, M. Hofmann, H. Ehrenberg, *Sci. Rep.* **2015**, *5*, 18380.
[44] M. Fleckenstein, O. Bohlen, M. A. Roscher, B. Bäker, *J. Power Sources* **2011**, *196*, 4769.
[45] P. Morales Torricos, C. Endisch, M. Lewerenz, *Batteries* **2023**, *9*, 230.
[46] X. Li, A. M. Colclasure, D. P. Finegan, D. Ren, Y. Shi, X. Feng, L. Cao, Y. Yang, K. Smith, *Electrochim. Acta* **2019**, *297*, 1109.
[47] J. Chen, M. N. Marlow, Q. Jiang, B. Wu, *J. Energy Storage* **2022**, *45*, 103669.
[48] D. Petz, M. J. Mühlbauer, V. Baran, A. Schökel, V. Kochetov, M. Hofmann, V. Dyadkin, P. Staron, G. Vaughan, U. Lienert, P. Müller-Buschbaum, A. Senyshyn, *Energy Storage Mater.* **2021**, *41*, 546.
[49] L. K. Willenberg, P. Dechent, G. Fuchs, D. U. Sauer, E. Figgemeier, *Sustainability* **2020**, *12*, 557.
[50] M. Lewerenz, J. Münnix, J. Schmalstieg, S. Käbitz, M. Knips, D. U. Sauer, *J. Power Sources* **2017**, *345*, 254.
[51] C. R. Birkl, M. R. Roberts, E. McTurk, P. G. Bruce, D. A. Howey, *J. Power Sources* **2017**, *341*, 373.
[52] I. Laresgoiti, S. Käbitz, M. Ecker, D. U. Sauer, *J. Power Sources* **2015**, *300*, 112.

Manuscript received: July 14, 2023
Revised manuscript received: October 2, 2023
Accepted manuscript online: November 12, 2023
Version of record online: December 8, 2023